T DELIVERY SVC
GITY
RD
44

ORDER NUMBER:	**CI-03381318-2**
Account Number:	FGH41316
Delivery Mode:	ARI
Delivery Address:	128.112.207.55
Submitted:	2002/12/12 15:05:41
Received:	2002/12/12 15:05:41
Printed:	2002/12/12 17:50:49

Periodical **WWW Catalogue** **UNITED STATES**

TN47375
FERROELECTRICS
00150193
166
1995
11-30
ELECTRIC FIELD INDUCED CRACKING IN FERROELECTRIC CERAMICS
C.S. LYNCH, W. YANG, L. COLLIER, Z. SUO ET AL.
IRN10127197
GORDON AND BREACH,
e: INNOPAC

e closed from December 24, 2002 at noon (ET) to January 2, am (ET).

st for this 20 page document: $10 document supply fee + $12 $22

Ferroelectrics, 1995, Vol. 166, pp. 11–30
Reprints available directly from the publisher
Photocopying permitted by license only

ELECTRIC FIELD INDUCED CRACKING IN FERROELECTRIC CERAMICS

C. S. LYNCH, W. YANG,† L. COLLIER, Z. SUO and R. M. McMEEKING
Department of Mechanical and Environmental Engineering, University of California, Santa Barbara, California 93106; †Department of Engineering Mechanics, Tsinghua University, Beijing 100084, China

(Received February 12, 1994; in final form September 16, 1994)

Ferroelectric ceramics are susceptible to fracture under high magnitude cyclic electric field. Flaws concentrate the electric field, inducing a large incompatible strain, and thereby a large stress. Stable growth of cracks with either conducting or insulating interiors is observed in 8/65/35 lanthanum lead zirconate titanate samples. Indentations on the electroded surface are filled with distilled water or a water-salt solution. Under cyclic electric field, tree like damage grows from the indented electrode. Indentations on the surfaces 90° to the electrodes are filled with silicone oil. This results in stable crack growth perpendicular to the cyclic electric field. Nonlinear fracture models are presented for both conducting and insulating cracks. Tensile stress intensity factors are predicted for both cases.

Keywords: Ferroelectric, PLZT, reliability, fracture, toughness, water treeing.

1. INTRODUCTION

After over forty years of development, perovskite type ferroelectric ceramics have found many applications. Their properties can be tailored by changing compositions and processing conditions, yet a problem persists that limits the device performance: ferroelectric materials degrade under repeated high magnitude electrical or mechanical loading sufficient to induce polarization switching. This paper is aimed at gaining a fundamental understanding of the reliability of ferroelectric ceramic materials and devices operating across switching thresholds. As with all brittle materials, reliability and fracture are intimately related. Fracture begins under mechanical loading if a flaw is larger than a critical size.

Stress concentrations at a crack tip can arise from either a mechanical or electrical load. McMeeking[1] demonstrated that when the interior of an elliptical cavity in a linear dielectric is conducting (insulating), the electric field intensifies at the crack tip if the applied field is parallel (perpendicular) to the flaw. In piezoelectric or electrostrictive materials, such an electric field also induces a strain field. This strain is constrained by the surrounding material, resulting in a stress field.

Pak,[2] McMeeking,[3] and Su *et al.*[4–6] have extended the concept of energy release rate to include electrical loading. Under electric field alone; a positive energy release rate is found for conducting cracks, and a negative energy release rate for insulating cracks. This implies that the insulating crack should not grow in a linear dielectric. For switchable ferroelectrics, however, we will show that a tensile stress intensity develops ahead of insulating cracks, causing cracks to grow parallel to the electrodes. Kramarov *et al.*[7] and Parton[8] have solved the linear-elastic, -piezoelectric, -dielectric fracture mechanics problem.

This paper first presents an experimental survey of the degradation of ferroelectric PLZT by stress fields, electric fields, and water corrosion. The magnitude of stress and electric field concentrations, induced by crack-like flaws, is sufficient to induce non-linear effects in PLZT. We therefore begin by performing a series of experiments to characterize the non-linear stress-strain-electric field behavior under uniform loading. Next, the mechanical fracture toughness is measured for use as a failure criterion under electrical loading, and crack tip stress fields are visualized using optical birefringence. Two types of electric field induced damage are examined: the cyclic growth of insulating cracks (Cao *et al.*,[9] Lynch *et al.*[10]), and electric field driven corrosion in the form of water treeing. The experimental results are used to develop a model that gives insight into the observed behavior of cracks during ferroelectric switching.

2. MATERIAL CHARACTERIZATION

The material chosen for this study is a relaxor ferroelectric; lead lanthanum zirconate titanate (PLZT) of composition La/Zr/Ti = 8/65/35, with a 5 μm grain diameter. This material was chosen for several reasons: it is transparent, and thus cracks are easily observed, it has the perovskite type crystal structure typical of most actuator materials, and its properties have been thoroughly investigated; see Haertling[11] for review. Table I lists properties of 8/65/35 PLZT. This composition is transparent in the unpoled and the slim loop states (described below), translucent in the poled ferroelectric state, and birefringent under strain or electric field. The electro-mechanical coupling in relaxor ferroelectrics is affected by stress, temperature, and electric field. High stress in the crack tip zone will either constrain or

TABLE I
Properties of PLZT[9]

Composition (La/Zr/Ti)	8/65/325
d_{33} (x10^{-12} C/N)	682
P^R (C/m²)	0.30
E_c (MV/m)	0.36
T_c (°C)	110
25°C Phase	Ferro. Rh.
ϵ_r	3350
tan δ (%)	2.5
resistivity (Ω-cm)	10^{13}
k	0.648
S_{11} (x10^{-12} m²/N)	12.4
Q_{11} (m⁴/C²)	0.018
Q_{12} (m⁴/C²)	-0.008

enhance switching, and energy dissipation under hysteretic cyclic loading generates heat. At low frequencies, thermal conduction results in a uniform temperature in the sample. At high frequency, the temperature is higher near the cracked region than in the bulk due to local electric field concentration causing large hysteresis. This causes strain mismatches due to local thermal expansion, and to the temperature and electric field dependence of the stress-strain-electric field constitutive relations. These considerations call for a general survey of nonlinear constitutive relations.

2.1 Effect of Temperature on Electric Field Induced Switching

Strain and polarization hysteresis loops are measured as a function of applied electric field at various temperatures. Electric displacement is monitored using the Sawyer-Tower circuit, and strain is measured with a surface mounted strain gauge. The samples are immersed in a silicone oil bath and the oil is heated. Temperature is monitored with a thermocouple. The applied electric field cycles between ± 1 MV/m. The effect of temperature on the properties of relaxor ferroelectrics is dramatic. No corrections were made to the strain data for thermal drift of the strain gauge.

Strain vs. Temperature. Figure 1 shows the measured longitudinal strain and electric displacement *vs.* the applied electric field (*S-E* and *D-E*) at several temperatures. At room temperature, 8/65/35 PLZT behaves as a normal ferroelectric ceramic with a butterfly hysteresis loop. As the temperature increases, the residual strain decreases and the minimum strain no longer occurs at a distinct point. At 42.3°C there is a range of electric field where the strain is at a minimum. This low strain state becomes stable relative to the high strain state as temperature increases. At 54°C the residual strain disappears and little hysteresis occurs in the *S-E* curve. As the temperature is further increased, the strain becomes nearly quadratic in electric field.

Electric Displacement vs. Temperature. At 23.4°C, 8/65/35 PLZT displays broad *D-E* hysteresis loops with a large residual electric displacement characteristic of ferroelectrics. At 42.3°C the *D-E* loops change shape. Starting at zero electric field, the initial increase of electric field removes the residual strain and polarization, driving the PLZT to a low strain state. This is seen as a jog in the *D-E* loop as it crosses zero electric displacement. When the coercive field is reached, the material is switched back into the high strain state with an accompanying jump in electric displacement. Above 75°C the hysteresis loops become slim (simultaneous with the emergence of the quadratic *S-E* behavior). At higher temperatures, the electric displacement varies linearly with the applied electric field. There is a slight jog in the electric displacement curves around $E = 0$ that disappears at 100°C, the temperature of the maximum in dielectric constant. Further temperature increase lowers the slope of the *D-E* curve and reduces the electrostrictive strain.

Optical Properties vs. Temperature. When cooled from high temperature to room temperature, hot pressed 8/65/35 PLZT is transparent. On application of the first electric field cycle at room temperature, the PLZT becomes translucent. In this

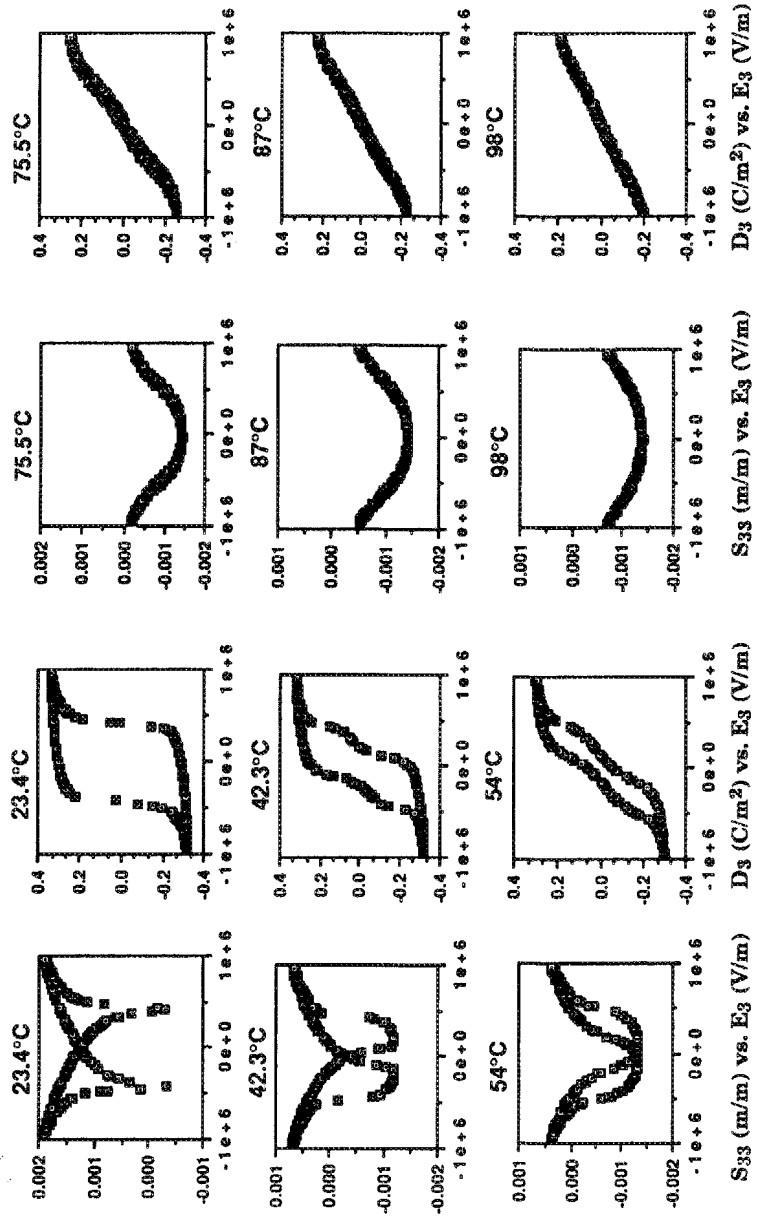

FIGURE 1 Temperature effects on the electro-mechanical response of 8/65/35 PLZT. At room temperature PLZT behaves as a ferroelectric. As the temperature is increased, there is a transition from piezoelectric to relaxor behavior.

state each grain of the ceramic has an optical axis aligned with its particular crystallographic orientation (birefringence). Light is refracted when passing from one grain to the next (due to the jump of refractive index), and is thus scattered as it passes through the sample. The birefringence is proportional to strain, thus the transmissivity changes as it is cycled around a polarization hysteresis loop. Maximum transmission occurs when the strain is the smallest (least distortion from a cubic structure). If the intensity of transmitted light is plotted against the applied electric field, the result looks like the *S-E* hysteresis loop. See Haertling[11] for a review.

2.2 *Effect of Stress on Electric Field Induced Switching*

Applied stress affects the coupling between electric field and strain in PLZT. When a mechanical force is applied along the long axis of the poled ceramic, the polarization can switch 90° with an associated large strain.

D-E and *S-E* loops are measured at room temperature as a function of uniaxial compressive stress applied parallel to the direction of polarization. A servo-hydraulic test frame applies a constant uniaxial stress. The strain is measured by monitoring the displacement and dividing by the specimen height. The constant load assures that there is no component of machine compliance in the displacement measurement. Figure 2 shows the effect of uniaxial stress on the *D-E* and the *S-E* behavior. (The room temperature *D-E* and *S-E* curves at zero stress are shown in Figure 1.)

Strain. At zero normal stress, the *S-E* curve has a characteristic butterfly shape. As the electric field is applied, a contraction strain is induced. When the coercive field is reached, the polarization switches, and the electric field now induces an expansion strain. When a uniaxial stress is applied in the direction of polarization, the stress attempts to switch the polarization 90° from the loading axis. As the electric field increases beyond the coercive field, the stress compresses the sample but the electric field extends it; the stress therefore hinders switching. See Figure 2. At a compressive stress of 5 MPa the coercive field no longer makes a sharp transition, and switching is completed over a range of electric field. The hysteresis loops look similar to those at a slightly elevated temperature. At 10 MPa the switching spreads further and the residual strain at zero electric field is lower. This effect is even more pronounced at 50 MPa: the applied electric field is now almost unable to switch the material against the applied stress. At 90 MPa the strain hysteresis loops are nearly gone.

Electric Displacement. The effect of compressive stress on electric displacement is less pronounced. The residual electric displacement diminishes with increasing stress, but there is still an open hysteresis loop at 90 MPa. It is interesting to note that at 90 MPa there is very little strain, yet still substantial polarization switching.

2.3 *Stress Induced Switching*

Ferroelectrics can undergo mechanical switching (ferroeleastic effect), Jaffe *et al.*,[13] and Cao *et al.*[14] We compare the stress-strain behavior of unpoled and poled samples

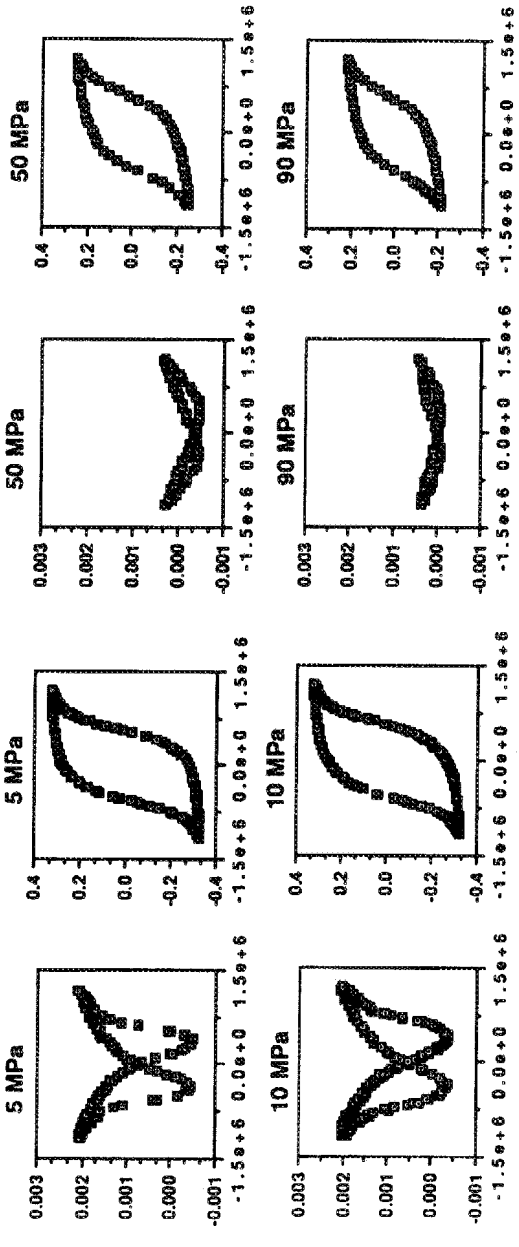

FIGURE 2 Stress effects at room temperature. An increase of stress in the direction of polarization reduces the piezoelectric strain and produces a mechanically assisted relaxation.

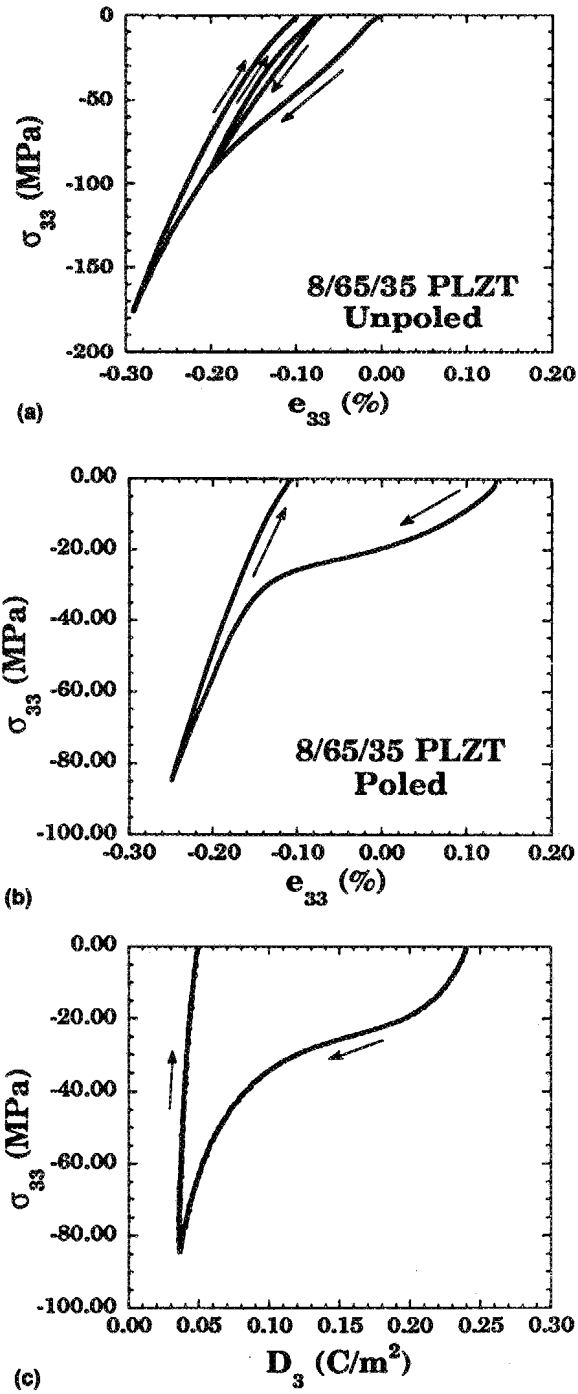

FIGURE 3 Stress-strain curves for (a) unpoled and (b) poled 8/65/35 PLZT. Mechanical switching occurs as stress is applied. This leaves a residual strain upon initial loading. The effect is greater in the poled material since initially there is more material with the correct orientation for mechanical switching. Figure 3(c) shows the electric displacement change corresponding to the test shown in Figure 3(b). A residual strain associated with mechanical switching results in a change in residual electric displacement.

to demonstrate the effect of mechanical switching. Figure 3 shows stress-strain and stress-electric displacement curves obtained at room temperature and zero electric field using polished 10 mm cubes. Strain is monitored with surface mounted strain gauges. The electric displacement is monitored during the stress-strain cycle using a Sawyer-Tower circuit. The stress rate on loading and unloading is 2 MPa per second.

Figure 3(a) shows the stress-strain curve for an unpoled sample. A load cycle is elastic if the load is small, but inelastic if the load is high. After the initial loading there is little additional residual strain. There is, however, a pronounced hysteresis loop during the cycle. The electric displacement remains unchanged from the unpoled state during the stress-strain cycle.

Figure 3(b) shows the stress-strain cycle for a sample poled in the direction of the applied uniaxial stress (load applied to the electrodes). The polarization switching gives a greater non-linear strain on initial loading, and a larger residual strain on unloading. In these experiments, the Wheatstone bridge signal conditioners for the strain gauges were zeroed with the material in the as cooled (not polarized) state. The initial strain shown in Figure 3(b) is therefore the remanent strain. The final strain after compressive loading is negative, corresponding to the 90° switched condition.

The electric displacement also changes irreversibly during mechanical loading of the poled sample. Figure 3(c) shows the stress plotted against the electric displacement for the test shown in Figure 3(b). As the stress increases, the electric displacement decreases. When the stress is removed there is a permanent change of electric displacement. The initial electric displacement is the remanent polarization. The compressive stress does not quite drive the polarization to zero.

The residual strain observed in the stress-strain curves is attributed to 90° switching. If a domain is aligned with its long axis in the direction of the compressive stress, it can ferroelastically switch 90° giving rise to a corresponding residual strain. The unpoled ceramic has a random orientation of domains. The poled ceramic has the polarization, and thus the long axis, aligned preferentially with the stress in the experiments. The poled material therefore has a greater volume of domains available for mechanical switching. This is consistent with the larger residual strain observed. The electric displacement also yields information about mechanical switching. The unpoled sample initially has zero net electric displacement. Since the domain orientation is random, half of the 90° switches come from positive oriented domains, and half from negative. There is therefore no net change in electric displacement. The poled sample initially has a residual polarization. 90° switching reduces this polarization.

3. CRACKS UNDER MECHANICAL LOADING

Our review of the mechanical and electrical behavior of 8/65/35 PLZT under homogeneous loading illustrates the coupled non-linearities associated with stress, polarization switching, and temperature. A deviation from homogeneous uniaxial stress results in the initiation of cracks. Flaws in ceramics present a natural source of inhomogeneous fields that can drive cracking. In this section we explore cracks in PLZT under mechanical loading.

3.1 *Center Crack*

In this set of experiments, a center crack in a thin panel of not poled PLZT is subjected to remote stress loading. PLZT is birefringent under strain or electric field. Mechanically induced birefringence is used to observe the crack tip strain field. Thin center cracked panels are viewed between crossed polarizers. Unpoled samples are sliced to 150 μm thickness and polished to 1 μm diamond. The samples are placed on a microscope slide and indented with a Vicker's indenter at a 2 N load. The thin samples buckle slightly and thus have a dominant crack across the center. The sampels are attached to a test frame between crossed polarizers with quarter wave plates (standard photo-elasticity set up), and viewed with a microscope. The process is recorded on video tape.

Birefringence is observed around the indentation prior to mechanical loading. As a uniaxial tensile stress is applied to the sample, the stress field at the crack tip begins to appear. This is seen in Figure 4(a). Further increase in tensile stress leads to stable crack growth. Figure 4(b) shows the sample just prior to the transition from stable to unstable crack growth. The shape of the stress concentration is clearly visible. Figure 4(c) shows the sample after fracture. The top and bottom half are separated. Residual birefringence appears around the indentation site, and in the wake of the stable crack, but not in the wake of the unstable crack.

Figure 4(d) is an SEM micrograph of the fracture surface near the indentation where residual birefringence is present. This region shows transgranular crack growth. Figure 4(e) is an SEM micrograph of a region away from the Vicker's indent where no residual birefringence occurred. This region shows intergranular crack growth.

The residual birefringence in the wake of the crack is attributed to ferroelectric switching. Ferroelastic switching is rate dependent, appearing as viscoelastic creep in stress-strain tests. During slow-stable crack growth there is sufficient time for switching to occur. During rapid-unstable crack growth there is no switching. These results suggest that ferroelastic toughening is present during slow crack growth, but not during fast growth.

3.2 *Fracture Toughness*

The fracture toughness of the PLZT in the not poled state is estimated by indentation data (Table II). The method of Anstis *et al.*[15] is used, namely

$$H = P/2a^2, \quad K_{Ic} = 0.016(Y/H)^{1/2}(P/c^{3/2}) \tag{1}$$

where H is the hardness, K_{Ic} the toughness, Y the Young's modulus, P the indent load, $2a$ the diagonal of the indented pyramid base, and $2c$ the total crack length. Crack lengths were measured immediately after the indentation to avoid slow crack growth. In computing the hardness and the toughness, we have used $P = 24.5$ N and $Y = 80.7$ GPa. The toughness so estimated is around 1 MPam$^{1/2}$.

4. ELECTRICAL CRACKS

Large displacement actuators are subjected to high electric fields. This can lead to cracking and dielectric breakdown even in the absence of mechanical load. In this

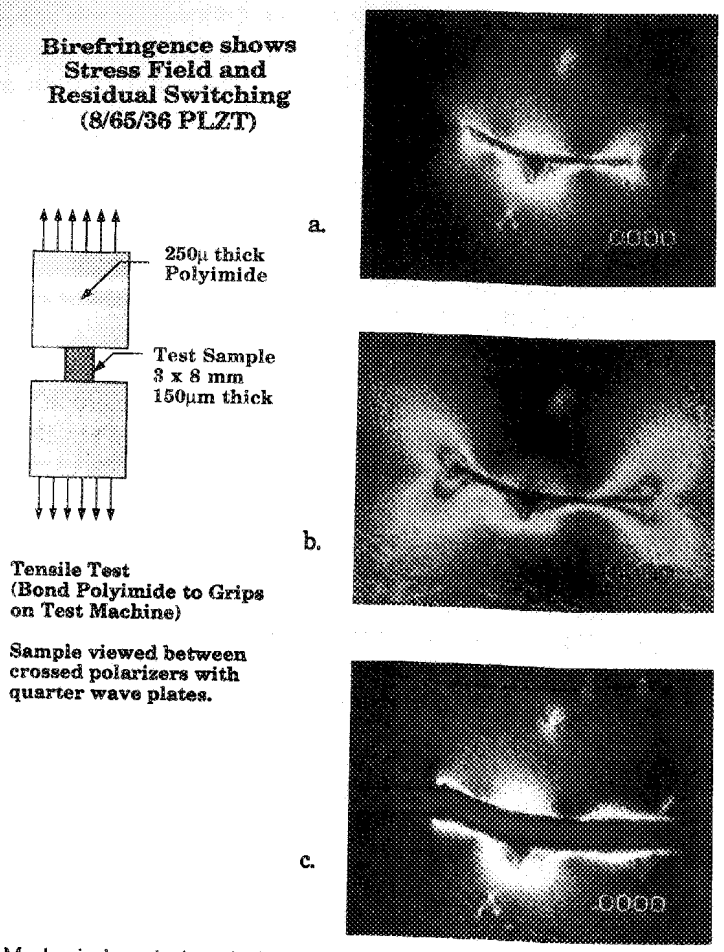

FIGURE 4 Mechanical cracks in uniaxial tension. (a) Birefringence shows the residual stress field in the center at the Vicker's identation and the effect of a small applied stress field shows as a stress concentration at the crack tips. (b) Increased stress increases the crack tip stress concentration and gives stable crack growth. (c) After failure there is residual birefringence in the wake of the stable crack growth but none in the wake of the rapid unstable growth. The two halves are separated. Width of field: 2 mm (d) SEM at the indentation site shows indentation damage zone to the left and transgranular crack growth to the right. (e) SEM away from the indentation shows intergranular crack growth. (See Color Plate I).

section we examine both insulating and conducting cracks in samples subjected to electrical loading.

4.1 Insulating Cracks

Insulating cracks are observed to grow, under cyclic electric field, perpendicular to the applied electric field about midway between the electrodes. Figure 5(a) shows the experimental arrangement. PLZT samples are cut to dimensions 2 × 3 × 20 mm^3 and the four larger surfaces polished to 1 μm diamond. A Vicker's indenter is placed in the center of a 3 × 20 mm^2 surface with a 24.5 N load. This

d.

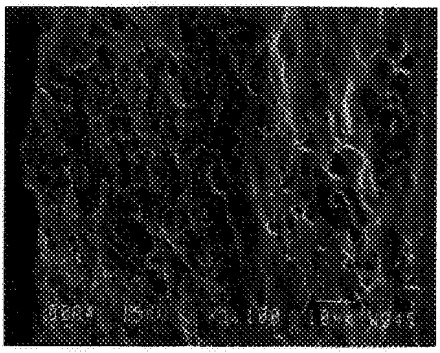

e.

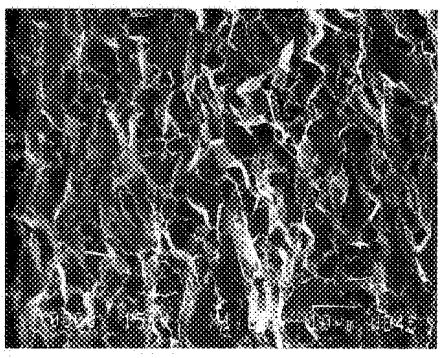

FIGURE 4 (*Continued*)

TABLE II
Vicker's indentation data

Test #	2a	2c	H	K_{Ic}
	(μm)	(μm)	GPa	MPa $m^{1/2}$
1	200	370	1.23	1.26
2	150	360	2.18	0.99
3	150	360	2.18	0.99
4	150	370	2.18	0.95
5	150	400	2.18	0.84
6	150	350	2.18	1.03
7	150	380	2.18	0.91

creates a square pyramid-shaped indentation about 150 μm across a base diagonal with cracks emanating from the corners; the total flaw size including the microcracks is around 380 μm. The cracks are aligned parallel and perpendicular to the electrodes. Silver epoxy electrodes are placed on the 2 × 20 mm^2 surfaces. The sample is dipped in silicone oil, connected to a Sawyer-Tower circuit, and cycled at 0.2

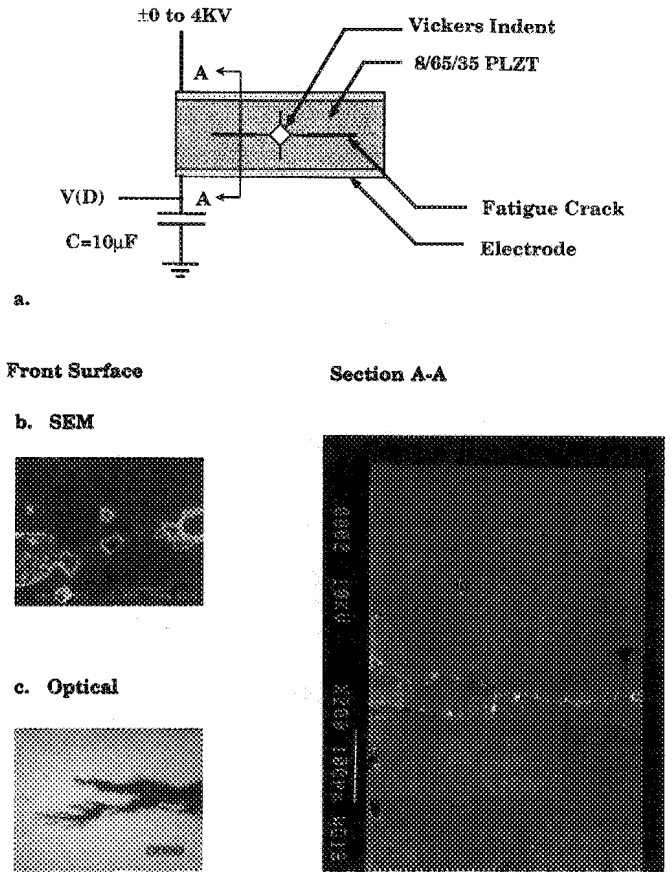

FIGURE 5 (a) Experimental arrangement for impermeable cyclic electric field fatigue cracks. (b) SEM of the intersection of the crack with the surface that shows the inter-granular character of the crack growth. (c) Optical micrograph of an impermeable fatigue crack in 8/65/35 PLZT. The crack has a wavy and bifurcated front that grows parallel to the electrodes. Width of field: 2 mm. (d) SEM of a cross section sliced through the crack. The crack bifurcates and is bridged in many locations.

Hz. The crack is observed through a microscope connected to a video camera. A scale is recorded to measure the crack length.

As the electric field is cycled, the crack opens and closes, giving an incremental growth. Opening occurs during polarization switching. At all other times the electric field drives the crack shut. Figure 5(b) is an SEM micrograph of the intersection of the crack and the surface. The crack propagates between grains. There is some chipping caused by the repeated opening and closing of the crack. Grains are clearly visible where chipping has occurred.

Figure 5(c) shows the crack in transmitted light. The crack bifurcates and has a feathered appearance, possibly due to a microcrack cloud around the crack tip. Figure 5(d) shows a cross section of the crack. The sample was sliced along A-A in Figure 5(a) and polished. There is a branch at the center of the sample. The crack is also bridged at numerous points. These cracks propagate completely through

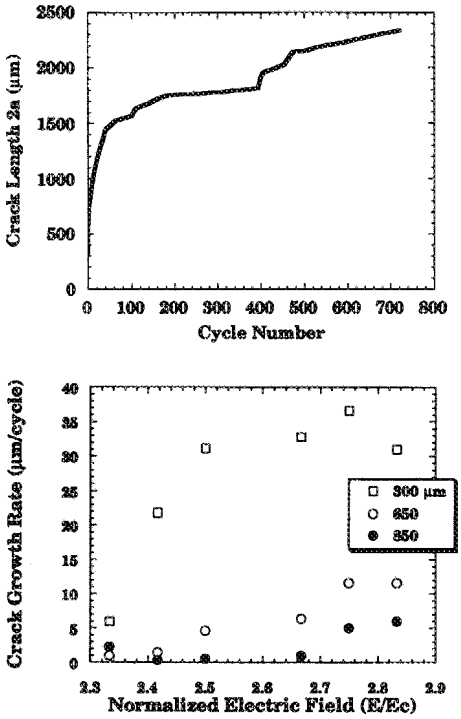

FIGURE 6 (a) Plot of crack length vs. cycle number. The distinct change in slope is associated with the geometry of the sample. This is believed associated with the transition from penny crack to center crack panel geometry. (b) Plot of initial crack growth rate vs. applied electric field demonstrates the dependence of crack driving force on electric field.

the sample, but will not separate the sample into two pieces. When the cracks become large, the *D-E* hysteresis loop is degraded.

Figure 6(a) plots crack length vs. cycle number. The crack grows rapidly in the initial stage and then slows down. Figure 6(b) plots growth rate as a function of applied electric field. Higher growth rates are obtained at higher electric fields. The initial growth rate can be as high as 35 μm per cycle. Several tests were performed at a frequency of 1.5 Hz and others at a frequency of 5 Hz. There was little frequency dependence of growth rate over this frequency range.

Three factors may contribute to the initial rapid growth, the residual stress field due to the indentation, a geometric effect, and toughening. Initially the growing crack is penny shaped and the crack length is small relative to the electrode separation distance. As the crack grows through the sample, the geometry changes from penny shaped to a center crack. Simultaneously, the crack length approaches the electrode spacing. Toughening may reduce the crack growth rate after some distance. When viewed in transmitter light the dark feathery appearance, shown in Figure 5(c), is seen. As the dark zone grows and bifurcates, the crack growth rate diminishes. Possible toughening mechanisms include microcracking, bifurcation, grain bridging, and ferroelastic switching. All of these mechanisms are active in 8/65/35 PLZT.

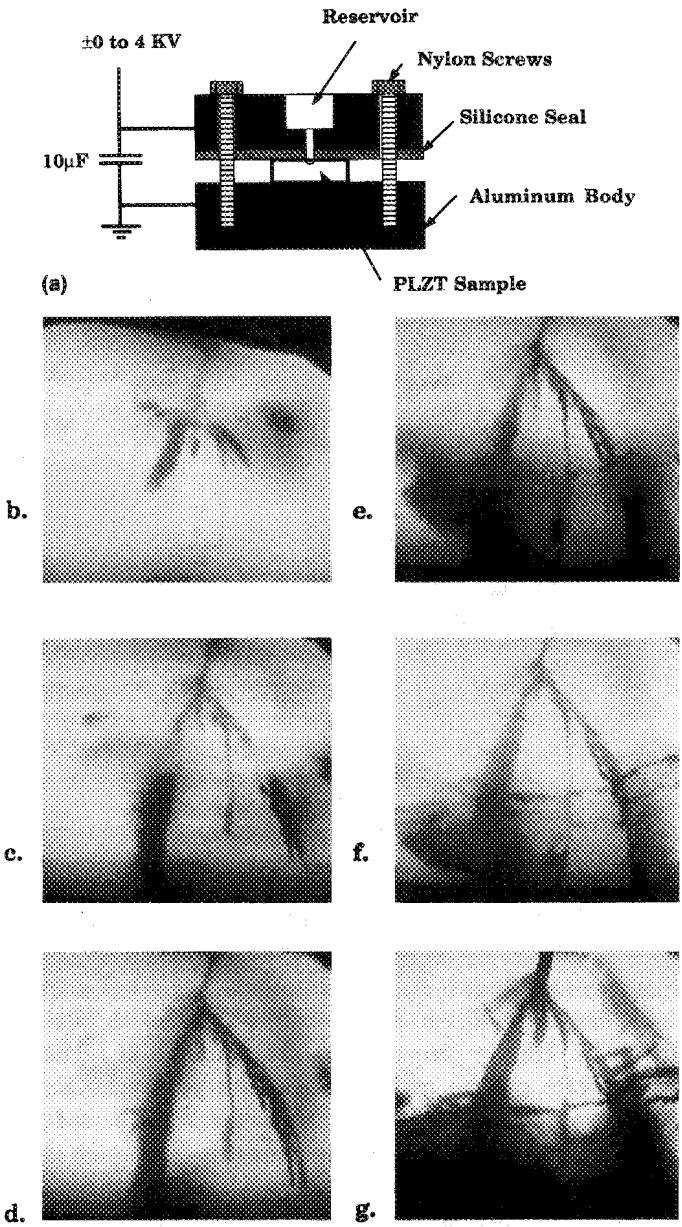

FIGURE 7 (a) Experimental arrangement for the growth of water trees and conducting crack paths. (b–d) A series of optical micrographs showing the development of the water tree structure. This treeing effect is seen for both salt water and distilled water. (e–g) A continuation of the series of micrographs showing the development of cracks from the tree structure. Width of field: 2 mm. (See Color Plate II).

4.2 Conducting Cracks

Figure 7(a) shows the experimental arrangement. A PLZT sample cut to dimensions of 2 × 3 × 10 mm^3 is polished on all faces. Au/Pd electrodes are sputtered to a thickness of 400 angstroms on the 3 × 10 mm^2 surfaces. A Vicker's indenter is placed in the center of the electroded surface with a 25 N load. The apparatus

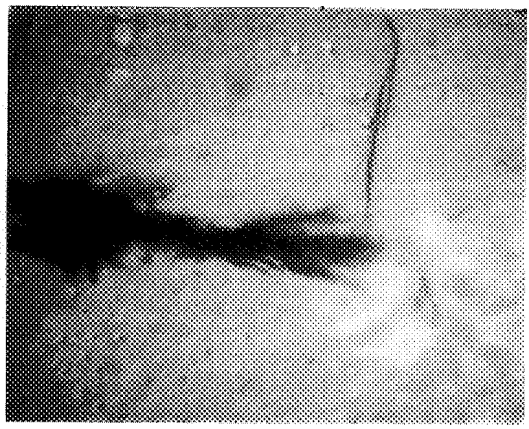

FIGURE 8 An optical micrograph of a tree like failure in the absence of a water source. The dark horizontal flaw started at the Vicker's indentation (left side) and was met by the conducting path that runs vertically down from the top (electrode). The conducting path is approximately 0.5 mm in from the surface. Width of field: 2 mm. (See Color Plate III).

shown is lightly clamped on the sample with the reservoir opening directly over the indentation. Either water or a salt water solution is placed in the reservoir. The electrodes are connected to a Sawyer-Tower circuit and the sample is cycled around a D-E loop at 0.2 Hz and $E/E_c = 2$.

When the reservoir is filled with either distilled water or an electrically conducting NaCl solution, a tree like structure grows into the sample. Figure 7 shows a series of micrographs of the sample viewed in transmitted light. The tree grows completely through the 2 mm thick sample in just ten or twelve cycles. The growth is cyclic and only occurs on the positive half cycle. In one test, with a conducting NaCl solution, a spider web like crack pattern developed as the tree approached the opposite electrode. This is seen in Figures 7(e–g).

The cyclic nature of the treeing and the rapid growth on one orientation of electric field suggest that the electric field aligns the dipolar water moelcules and helps transport them toward the opposite electrode. The electric field may even contribute to driving a corrosion reaction between the water and the oxide.

We have observed treeing, in the absence of a water reservoir, in samples cycled close to the breakdown field. Figure 8 shows an optical micrograph of an impermeable crack tip in transmitted light. Note the tree like structure that grows down from the electrode to the crack tip. This tree resulted in arrest of the insulating crack. When a tree reaches the opposite electrode, a short circuit results.

5. THEORETICAL CONSIDERATIONS

The experimentally observed material behavior is described with a mechanics model developed by Yang and Suo.[16] A model that predicts all details of the experimental observations should incorporate the observed non-linearities in stress, electric field, and temperature, and simultaneously solve all of the coupled field equations. This will require the development of new constitutive laws and extensive numerical analysis. The model presented here is based on step like switching and ignores the

effect of stress on electric field. Although many features of the material behavior have been left out, this model captures the essence of the switching behavior and gives insight into the source of the stress field that drives crack growth.

The model is constructed in several steps. The coupling of stress to electric field is ignored so that the electric potential is governed by Laplace's equation. The interior of the crack is either conducting or impermeable to electric field. The switching problem is simplified by considering steplike electrostriction in which, in the absencce of stress, the strain is zero when $E < E_c$ and γ_s when $E > E_c$. Since the electric field is concentrated around a crack tip, switching is assumed to take place in a zone around the tip, bounded by radius R, within which $E > E_c$. The switching strain is not compatible unless there is a stress field present. The material within the zone bounded by R attempts to undergo switching strain, but is constrained by the surrounding material. The constraining stress, strain, and displacements are represented by the general solution to the biharmonic equation (linear elasticity). Matching of the solutions at the interface $r = R$ yields the full stress, strain, and displacement fields.

The calculated fields are produced by a thin planar layer of conducting or impermeable material perturbing the electric field. There are tractions on this layer that must be removed so the layer will represent the free surfaces of a crack face. The tractions on the crack surface are negated by opposite tractions. The negating tractions produce a wedging force that drives the crack open. This results in a tensile mode I stress intensity factor.

5.1 *Steplike Electrostriction*

An inhomogeneous biharmonic equation governs the steplike electrostriction problem. The governing equation is supplemented by the continuity requirements of traction and displacements at $r = R$, the boundary between the switching zone and the surrounding elastic material. A closed form solution for the abovementioned problem is derived, which leads to the following expression for hoop stress near a plane of impermeable material.

$$\sigma_{\theta\theta} = -Y'\gamma_s \left[\frac{1 - (1 + 2\nu)q}{4} + \frac{(1 + q)}{3} \cos\theta \right] \quad \text{for } r < R \tag{2}$$

$$\sigma_{\theta\theta} = Y'\gamma_s \left[\frac{1 - (1 + 2\nu)q}{4} \frac{R^2}{r^2} + \frac{(1 + q)}{3} \frac{R^3}{r^3} \cos\theta \right] \quad \text{for } r > R \tag{3}$$

Where Y' is the plane strain Young's modulus, γ_s is the switching strain, and q is the ratio of electrostrictive coefficients $(-Q_{12}/Q_{11})$. Figure 9 describes the angular variation of the switching in the vicinity of an impermeable crack, where θ denotes the polar angle, and shows the stress distribution along the crack plane caused by the switching.

5.2 *Small Scale Switching*

Attention is focused on the situation when the size of switching region is small compared to the other characteristic lengths. The same qualitative features would

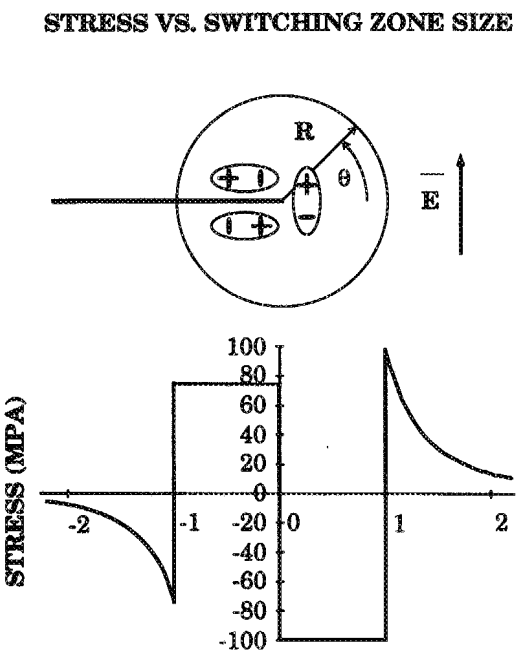

FIGURE 9 Switching near the top of an impermeable sheet and the associated stress field on the plane of the sheet.

emerge for the case of large scale switching. Figure 10 shows how the small scale switching analysis around a crack is decomposed into the superposition of the electrostriction problem (with the crack faces joined together) and a traction negating problem to restore the free surface condition along the crack faces. The electrostriction problem with joined crack faces does not have a singularity as r approaches zero and thus does not contribute to the stress intensity factor. The traction negating problem gives rise to the singularity.

5.3 *Stress Intensity Factors*

The stress intensity factor K_I is found by integrating a distributed wedge force from a-R to a, where a is the crack length.[17] The intensity of the wedge force is found from Equation 7 with $\theta = \pi$. Taking $\nu = 0.33$ and $q = 0.44$ gives

$$\sigma_{\theta\theta} = .42Y'\gamma_s \tag{4}$$

and

$$K_I = 2\sigma_{\theta\theta}\sqrt{\frac{a}{\pi}}\arccos\left(\frac{a-R}{a}\right) \tag{5}$$

When the crack is small relative to the sample dimensions, the size of the switched zone is limited by the size of the flaw. The electric field concentrations at each

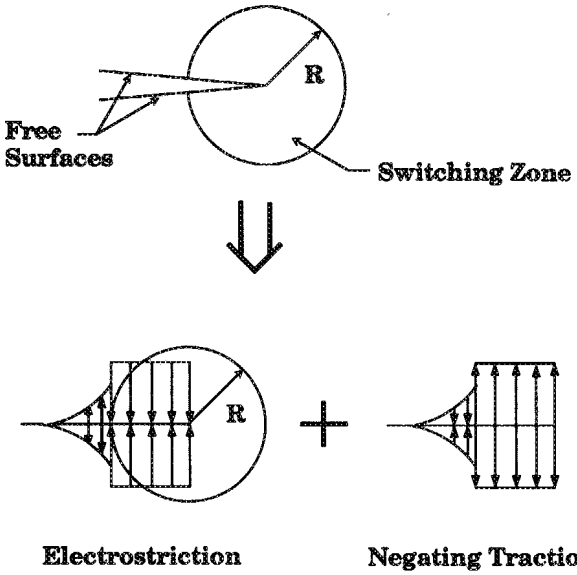

FIGURE 10 A superposition scheme in which an electric fracture problem is decomposed into an electrostriction problem and a traction negating problem. The stress field on the surfaces of the sheet in Figure 9 are negated with wedging forces to form the free surfaces of a crack. The wedging forces give a mode I stress intensity factor.

crack tip diminish toward the center of the crack. We therefore estimate the maximum ratio of R/a as 1/2. This gives

$$K_I = \frac{2}{3}\sigma_{\theta\theta}\sqrt{\pi a} \tag{6}$$

The stress intensity increases as $a^{1/2}$. The initial value is found from $2a = 400\ \mu m$, $Y' = 90$ GPa, $\gamma_s = 0.002$, and $R = a/2$. This gives $K_I = 1.3$ MPam$^{1/2}$. The stress intensity increases as the crack grows.

When the crack length approaches the thickness of the sample, the size of the zone of high electric field is constrained by the proximity of the electrodes. When the crack is small relative to the sample dimensions, the wedging force at each crack tip contributes to the stress intensity at the opposite tip. When the crack length becomes comparable to the thickness of the sample, the switching zone size can no longer increase while the crack continues to grow. The effect of the wedging on the opposite tip therefore diminishes. This is consistent with the decrease in crack growth rate when the crack length approaches the sample thickness. See Figure 6. The real material does not really undergo step like electrostriction. The magnitude of the electrostrictive strain is a function of both the electric field and the stress field. The effect of constraining stress on switching was discussed in section 2. An applied field just above the coercive field will cause less switching than one several times the coercive field. This effect is seen in the increase of growth rate at higher electric field shown in Figure 6(b). The remaining question is, why is the crack growth cyclic?

5.4 Crack Arrest and Cyclic Growth

The model we have presented is for an idealized impermeable crack. If we consider a permeable elliptical crack in a linear dielectric, the conditions of a continuous component of electric displacement normal to the crack/matrix interface and a continuous component of electric field tangential to the interface result in an electric field intensification within the crack in a semi-infinite solid that is approximately proportional to the ratio of the permittivity of the matrix material to that of the crack interior. This gives an extremely high electric field within the crack. The electric field within a crack of elliptical cross section is uniform. The intensified field is thus found in the matrix material at the crack tip. The strain-electric field coupling gives both large strain energy density and large electric energy density in the crack tip zone.

The amplification of electric field within the crack is on the order of 3000 times for this material. This substantially exceeds the dielectric breakdown field of either air or silicone oil. This effect was examined by slicing a sample midway between the electrodes and polishing the surfaces. The polished faces were placed together and then the sample was bonded to the platens of a test frame. The test frame was placed in displacement control and the halves were separated to produce a gap of 50 μm. An electric field was applied. As the electric field passed through the coercive field, blue sparks occurred in the gap. Reduction of the field to zero followed by reloading did not induce much sparking. Reversal of the field, however, produced additional sparking at the coercive field. The largest amount of electrical discharge within the gap is associated with the polarization reversal.

To account for the cyclical nature of electric field driven crack growth, we postulate that, under a strong electric field, a crack grows within a perovskite-type ceramics such that it separates the crystal lattice with a residual charge distribution. This charge distribution on the newly formed crack surfaces will reduce the electric energy stored within the crack by terminating the electric displacement. This will, in turn, reduce the strain energy stored in the crack tip zone. As the new crack surface forms, the local stress intensity will diminish. Upon reversal of the electric field, the surface charge distribution will now add to the electric displacement and enhance the crack tip field. Again, as new crack surface forms, an opposite surface charge separation will form and diminish the crack tip field. The process repeats itself, giving cyclic crack growth.

6. CONCLUDING REMARKS

Electrical fatigue cracks propagate in ferroelectric PLZT under cyclic electric field loading above the coercive field. Crack growth rate increases with electric field and decreases with crack length. The decrease is shown to be a geometric effect possibly coupled with a toughening effect. Several potential toughening mechanisms are identified, including transformation, bifurcation, microcrack cloud formation, and grain bridging. A mechanics model is proposed for electric fatigue crack propagation that captures the essential features of the cyclic crack growth. An electric field concentration at the crack tip induces a large local strain. This strain is con-

strained by the surrounding material. The resulting stress intensity factor is larger than the measured mechanical fracture toughness, leading to crack propagation.

A model that explains the cyclic nature of the electric crack propagation is proposed. If the electric displacement is continuous from the matrix into the crack, there is a large electric field within the crack and a strain energy concentration in front of the crack. This energy is reduced if there is a surface charge distribution over the crack surface that reduces the electric field concentration. If, as the crack propagates under a strong electric field, the atomic bonds separate so as to leave a net surface charge distribution, the energy of the system will be reduced and the crack will arrest. When the field is reversed, the surface charge distribution will enhance the crack tip field and the process will repeat.

Experiments designed to study the behavior of conducting cracks resulted in the observation of an unexpected phenomenon, water treeing. This is apparently electric field driven corrosion.

ACKNOWLEDGEMENTS

This work was supported by ONR through contract N0014-93-1-0110 and N0014-931-0200, and by NSF through a Young Investigator Award MSS-9258115 for Z. Suo.

REFERENCES

1. R. M. McMeeking, "Electrostrictive Stress Near Crack-like Flaws," *J. Appl. Math. Phys.*, **40,** 615–627 (1989)
2. Y. E. Pak, "Crack Extension Force in a Piezoelectric Material," *J. Appl. Mech.*, **57,** 647–653 (1990).
3. R. M. McMeeking, "A J-Integral for the Analysis of Electrically Induced Mechanical Stress at Cracks in Elastic Dielectrics," *Int. J. Engrg. Sci.*, **28,** 605–613 (1990).
4. Z. Suo, C.-M. Kuo, D. M. Barnett and J. R. Willis, "Fracture Mechanics for Piezoelectric Ceramics," *J. Mech. Phys. Solids*, **40,** 739–765 (1992).
5. Z. Suo, "Models for Breakdown-Resistant Dielectric and Ferroelectric Ceramics," *J. Mech. Phys. Solids*, **41,** 1155–1176 (1993).
6. Z. Sou, "Mechanics Concepts for Failure in Ferroelectric Ceramics," *Smart Structures and Materials*, AD-Vol. 24/AMD-Vol. 123, ASME (1991).
7. S. O. Kramarov, A. A. Kuprienko and N. Egorov, "Influence of the Piezo Effect on the Crack Growth in Crystals with the Perovskite Structure," *Sov. Phys. Solid State*, **29,** 705–6 (1987).
8. V. Z. Parton, "Fracture Mechanics," Gordon and Breach," N.Y. (1992).
9. H. C. Cao, M.-Y. He and A. G. Evans, "Electric Field-Induced Fatigue Crack Growth in Ferroelectric Ceramics," submitted for publication (1993).
10. C. S. Lynch, L. Chen, W. Yang, Z. Suo and R. M. McMeeking, "Crack Growth in Ferroelectric Ceramics Driven by Cyclic Polarization Switching," in *Adaptive Structures and Materials Systems*, Ed. G. P. Carmen and T. E. Garcia, ASME AD-V35 (1994).
11. G. H. Haertling, "PLZT Electrooptic Materials and Applications—A Review," *Ferroelectrics*, **75,** 25–55 (1987).
12. Z. Y. Meng, U. Kumar and L. E. Cross, "Electrostriction in Lead Lanthanum Zirconate-Titanate Ceramics," *J. Am. Ceram. Soc.*, **68,** 459–462 (1985).
13. B. Jaffe, W. R. Cooke and H. Jaffe, *Piezoelectric Ceramics* (Academic Press, London and New York), pp. 83–85 (1971).
14. H. Cao and A. G. Evans, "Nonlinear Deformation of Ferroelectric Ceramics," *J. Am. Ceram. Soc.*, **76,** 890–96 (1993).
15. G. R. Anstis, P. Chantikul, B. R. Lawn and D. B. Marshall, "A Critical Evaluation of Indentation Techniques for Measuring Fracture Toughness: I, Direct Measurements," *J. Am. Ceram. Soc.*, **64,** 533–538.
16. W. Yang and Z. Suo, "Cracking in Ceramic Actuators," *J. Mech. Phys. Solids*, accepted for publication (1993).
17. D. Broek, "Elementary Engineering Fracture Mechanics," Martinus Nijhoff Publishers (1986).